Progress In Electromagnetics Research M, Vol. 101, 149–159, 2021

Resonator Based Antenna Sensor for Breast Cancer Detection

Praveen K. Rao* **and Rajan Mishra**

Abstract—A compact ultra-wideband antenna is presented for detecting malignant cells in the breast. The dimension of the proposed circular resonator-based antenna is 20 mm × 30 mm × 1.6 mm. The antenna sensor operates within the 3.1 GHz to 6.8 GHz (105.71%) range with peak gain 4.8 dB, radiation efficiency 89.2%, and an omnidirectional radiation pattern. Three types of breast phantoms (i.e., phantom without tumor, a phantom with a single tumor, and phantom with two tumors) are also fabricated. The electrical properties of the malignant cells differ from non-malignant breast cells. *S*-parameters have been measured with phantom, then with the help of Principal Component Analysis (PCA), and normal and malignant breast phantoms are identified. Further, the tumor's locations in the breast phantom are find out by using the specific absorption rate (SAR) values.

1. INTRODUCTION

As per the World Health Organization report, breast cancer is a leading cause of death among women worldwide. 2.1 million new cases of breast cancer are added every year. It is due to malignant or tumor cells present in the breast tissues [1]. The major factor in the treatment of breast cancer is a reliable diagnosis at an early stage. Early detection can achieve a survivability rate of 97% for breast cancer [2]. X-ray mammography, computed tomography (CT) scan, magnetic resonance imaging (MRI), ultrasound are commonly used to detect breast cancer [3]. These methods have various disadvantages. X-ray is a painful, ionizing process and has very low capability to detect cancer at an early stage. MRI and ultrasound are non-ionization methods, and they are expensive and unable to detect cancer symptoms at an early stage [4].

Microwave sensing is the most attractive technique for the early detection of breast cancer. It is a comfortable, harmless, cheap, and non-invasive method [5, 6]. In this method, a radiation form antenna sensor is incident on the object. Since cancerous tissues have higher permittivity than healthy tissues, the scattering of microwaves is increased. Current research on microwave sensing in the last decade has grown exponentially [7, 8]. An antenna sensor is the key component of a microwave sensing device. The system sensing capability can be improved by designing an efficient UWB antenna sensor with high gain, high radiation efficiency, and stable radiation pattern. [9]. Several initial works have also been reported on malignant tumor detection and studied multi-layered breast phantom models [10, 11]. It is well known that the UWB spectrum lies from 3 GHz to 11 GHz range, and it is also noticed that certain other spectrum values fall within this range. These frequency bands construct an inevitable overlap in UWB communication systems that affect frequency bands corresponding use for utilization such as microwave imaging applications [12, 13]. It is widely known that the corresponding range is created by introducing slot resonators within the reference antenna such as complementary split-ring resonators and fractal-based different proposed resonators [14, 15]. Defected ground, parasitic resonators, filter integration, and matching stubs within the reference antenna are also some other techniques that are extensively investigated [16–18]. It is expensive and complex to use microwave imaging techniques.

Received 11 January 2021, Accepted 10 February 2021, Scheduled 1 March 2021
* Corresponding author: Praveen Kumar Rao (rao.praveenmmmut@gmail.com).
The authors are with the Department of Electronic and Communication Engineering, Madan Mohan Malaviya University of Technology, Gorakhpur, India.

For breast cancer detection, several types of antennas have been reported, such as the cross-Vivaldi antenna [19], unit cell antenna [20], slot antenna [21], metamaterial-based antenna [22], and switchable filter antenna [23]. These reported systems have many radiating elements. The antenna design for an efficient system should be compact and wideband with high radiation efficiency. Malignant tissues have a tendency to absorb more power than normal tissues. Therefore, malignant tissues have more SAR. In [24–26], SAR investigation is reported using a UWB antenna sensor for breast cancer detection.

The proposed work focuses on the design of a compact circular resonator antenna for breast cancer detections. The proposed sensing technique is based on the fact that the material adjustment of a woman's two breasts (left and right) is commensurable. The detection process consists of two similar sensors for testing both left and right breasts concurrently. Then the reflection coefficients of the two sensors are analysed using Principal Component Analysis (PCA) for tumor detection. Further, the tumor's location is identified by using SAR values, and SAR values are less in the normal phantom than tumorous phantom. Table 1 describes the advantages of the proposed breast tumor sensor compared to the existing reported MI sensors. The antenna sensor consists of a single antenna element with a single feed point, which reduces the size, complexity, and cost of the device compared to devices having antenna sensors consisting of multiple radiating elements. The antenna sensor offers an omnidirectional radiation pattern, which leads to improving the sensor's sensitivity. Therefore, the sensor provides full coverage of the breast. So there is no need for mechanical motors to shift the sensor throughout the breast.

Table 1. Comparison between reported sensor and proposed sensor.

Feature	Reported sensors	Proposed Sensor
Number of elements	Multiple sensor with multiple feed	One sensor with one fed
Time of Testing	More time for setup and processing	Few seconds
Simplicity	Complicated processing and Complex system	Simple testing and simple system
Portability	Most of MI systems are bulky	Portable

2. ANTENNA DESIGN AND ANALYSIS

The proposed antenna is designed on an FR-4 epoxy glass (dielectric constant = 4.4, loss tangent = 0.02, and thickness = 1.6 mm) substrate with double-sided copper coating. A feed-line and modified rectangular patch configure the top surface of the substrate. A circular resonator is printed on the substrate's backside, and there is a thin strip that links the circular resonator to the partial ground

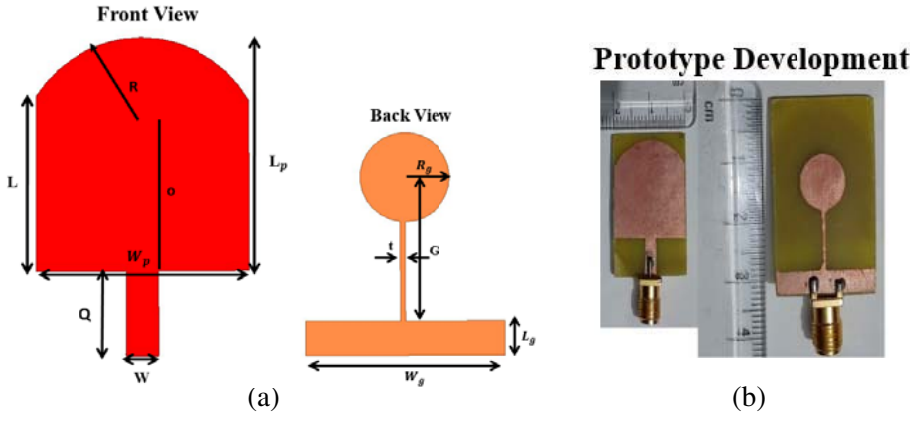

Figure 1. (a) Geometric of proposed antenna, (b) layout of antenna.

Table 2. Dimensions (millimetres) of proposed antenna.

Parameter	L_p	W_p	W	P	W_g	o	L_g	G	R_g	t	Q	R
Value (mm)	22	20	3	15	20	17	3.5	14	4.5	0.5	8	10

plane, as shown in Figure 1(a). Dimensions of the antenna are tabulated in Table 2.

The equivalent circuit of proposed antenna sensor is shown in Figure 2. L_u indicates the series impedance due to the patch of the antenna. The circular resonator, which forms the parallel L_g and C_g tank circuit, is another substructure of the proposed antenna.

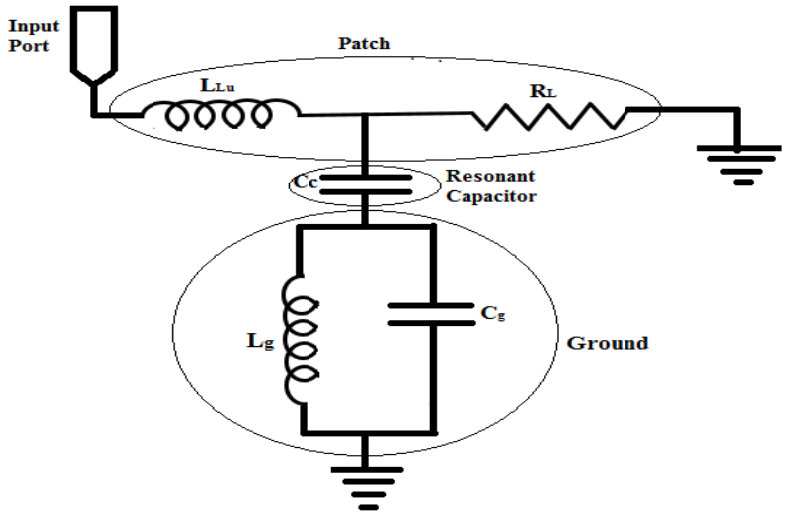

Figure 2. Equivalent circuit diagram of proposed antenna.

C_c is the coupling capacitor between the patch and ground plane. The adjacent cells of circular resonator are coupled electrically, while the typical design based on the resonator in the ground plane considers only the electric coupling [27, 28]. The equivalent circuit diagram is similar to the equivalent circuit diagram of the negative epsilon transmission line. So, the dispersion relationship can be achieved using the Bloch-Floquet theorem's [29] periodic boundary conditions.

$$\beta d = \cos^{-1}(1 + ZY/2) \tag{1}$$

where Z = series impedance, Y = shunt impedance, and d = unit cell length of the proposed antenna.

$$Z = (j\omega L_u), \text{ and } Y = (j\omega C_c) / (j\omega C_g + 1/j\omega L_g)$$

Shunt parameters must control the ZOR frequency since the designed antenna is configured with open-ended boundary conditions. The values of Z and Y are substituted in Eq. (1) [29].

$$\beta d = \cos^{-1}\left(1 + \frac{\left(\frac{\omega^2}{\omega_p^2}\right)\left(\frac{\omega^2}{\omega_q^2}\right) - \left(\frac{\omega^2}{\omega_p^2}\right)}{2\left(1 - \left(\frac{\omega^2}{\omega_r^2}\right)\right)}\right) \tag{2}$$

where

$$\omega_p = \frac{1}{\sqrt{L_u C_c}}, \quad \omega_q = \frac{1}{\sqrt{L_g C_g}}, \quad \text{and} \quad \omega_r = \frac{1}{\sqrt{L_u (C_g + C_g)}} \tag{3}$$

Further, the resonant mode can also be calculated by Eq. (3)

$$\beta d = n\pi \tag{4}$$

where n indicates the number of modes.

To calculate ZOR mode, the value of n should be zero, which means no phase variation throughout the patch. From Eqs. (2) and (3) at ZOR mode, the ZOR frequency is given by in Eq. (4).

$$w_z = w_{zoR} = \frac{1}{\sqrt{L_g C_g}} \tag{5}$$

It is clear that the ZOR frequency can be controlled by varying the shunt parameters (L_g and C_g).

Figure 3(a) shows the design process of the antenna sensor. The antenna, without a circular resonator and thin strip, gives a bandwidth of 3.4 GHz to 5.5 GHz. The antenna with a circular resonator and thin strip offers an improved bandwidth at the frequency of 2.6 GHz.

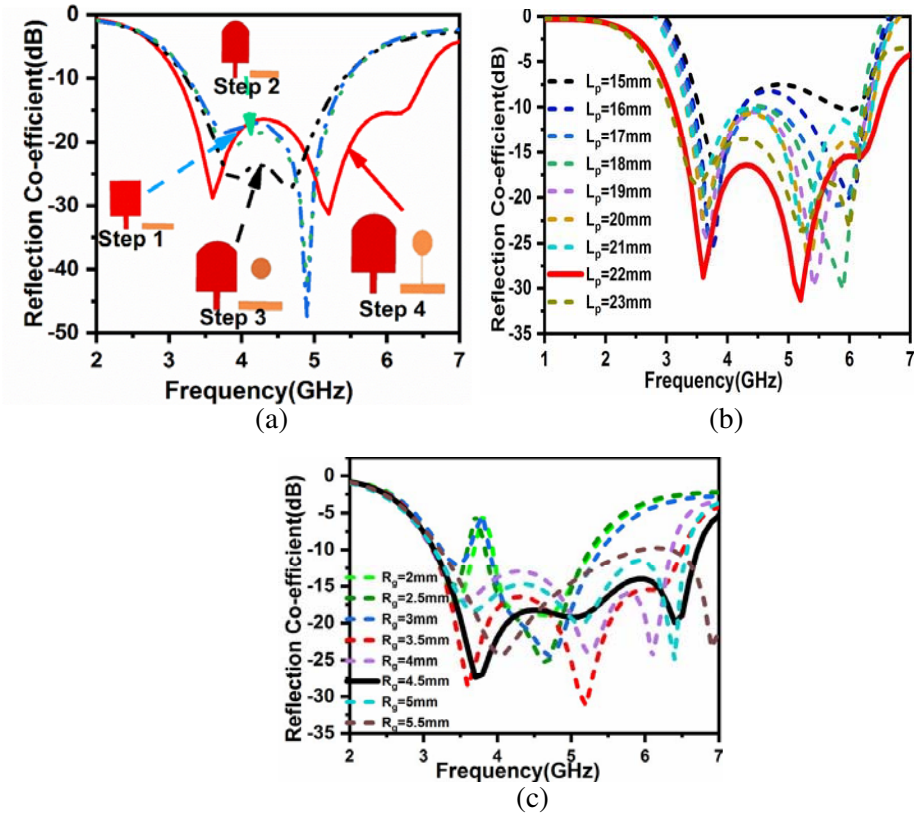

Figure 3. (a) Antenna evolution of reflection coefficient, (b) parametric analysis of patch length, (c) parametric analysis of circular resonator radius.

The antenna performance is mainly dependent on patch lengths that vary from 15 mm to 23 mm, as shown in Figure 3(b). At patch length, $L_p = 22$ mm, the optimized antenna performance has been obtained. Figure 3(c) shows the variation of circular resonator's radius from 2 mm to 5 mm. It is clearly indicated that the reflected power and bandwidth are reduced when the circular resonator radius is less than 3 mm.

3. RESULT

Figure 4(a) shows the simulated and measured reflection coefficients of the antenna. The antenna offers bandwidth from 3.1 GHz to 6.8 GHz. It is a good agreement between the simulated and measured results. Figure 4(b) shows simulated and measured gains and radiation efficiencies of the antenna. It offers peak gain of 4.8 dB with an average radiation efficiency of 89.2% over the 3.1 GHz to 6.8 GHz frequency range.

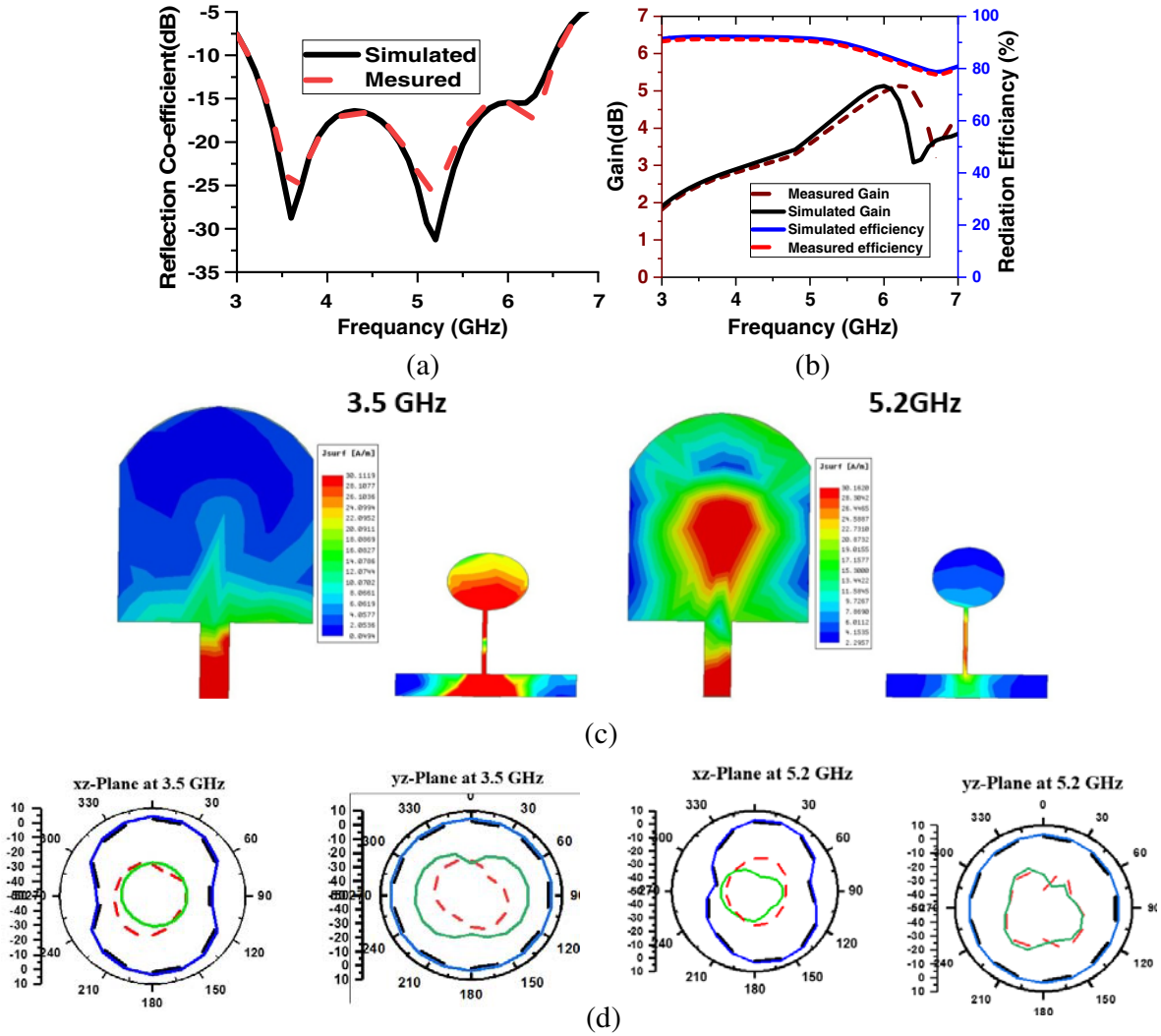

Figure 4. Simulated and measured, (a) reflection coefficient of proposed antenna, (b) gain and efficiency of the proposed antenna, (c) current distribution at 3.5 GHz and 5.2 GHz, (d) simulated and measured radiation pattern at 3.5 GHz in xz-plane and yz-plane, and at 5.2 GHz in xz-plane and yz-plane.

The current distribution is shown in Figure 4(c) for both the resonance peaks at 3.5 GHz and 5.2 GHz. This indicates that at 3.5 GHz frequency, radiation occurs mainly from the circular resonator, while at 5.2 GHz, maximum radiation occurs due to the center part of the patch.

The measured and simulated co-polarized and cross-polarized radiation patterns are shown in Figure 4(d). The proposed UWB antenna sensor provides a consistent omnidirectional radiation pattern for both the resonance peaks.

4. BREAST PHANTOM DEVELOPMENT AND TUMOR DETECTION PROCESS

The breast phantom model consists of four layers (Skin, fat, glandular, and muscular). The breast phantom model is simulated using HFSS, and the malignant tumors are introduced in the breast's innermost layer at different locations, as shown in Figure 5(a). The tumor is introduced at different locations at different times instant to detect the tumor within the breast phantom. The phantom model is simulated for 3.5 GHz solution frequency. The heterogeneous phantom model is developed using polyethylene powder, propylene glycol, formalin sodium chloride, NaCl, agar powder, xanthan gum, detergent, and distilled water. Three phantom models have been developed for experimental, i.e.,

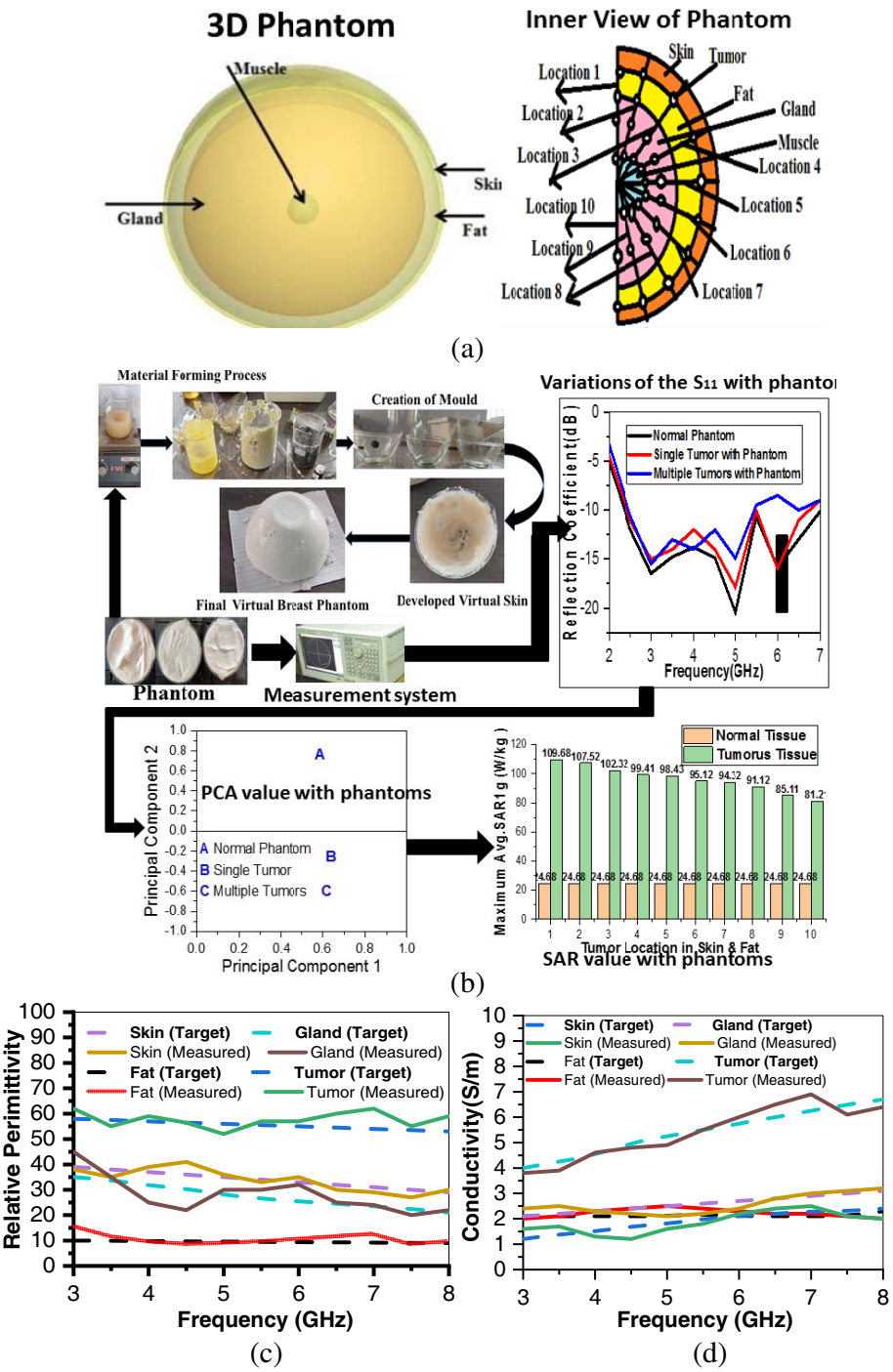

Figure 5. (a) Simulated breast model (skin 70 mm, fat 60 mm, gland 60 mm and muscle 5 mm) and inner section of breast, (b) fabrication process and prototype of breast cancer detection, (d) relative permittivity of target and measured heterogeneous phantom, (e) conductivity of target and measured heterogeneous phantom.

homogeneous normal phantom, homogeneous phantom with single tumor, and homogeneous phantom with two tumors. The fabrication process [30] of the phantom model setup and prototype of breast cancer detection is shown in Figure 5(b).

Dielectric constant and loss tangent measurement are performed by using a 85070E dielectric sample

kit and vector network analyzer (VNA). In the experiment, six data samples for different layers at different locations are used to obtain electrical properties of breast phantom. The average value of these six data samples are very close to the target value. The relative permittivity and conductivity graph of these layers are shown in Figures 5(c) and 5(d). The skin, fat tissue, gland tissue, and tumor tissue layers have dielectric ranges of 34–40, 9–14, 18–45, and 60–61, respectively. The skin, fat tissue, gland tissue, tumor tissue layers have a conductivity in ranges of 1.5–2.5, 1.7–2.5, 1.5–4 Siemens per meter (S/m), respectively.

4.1. PCA Analysis of Reflection Coefficients

Antenna's return loss is obtained by putting the antenna on top of the simulated breast phantom. Further tumor is inserted between fat and glandular layers at various locations from location 1 to location 9 which is shown in Figure 6(a). After that PCA is obtained at various data of S_{11} with the help of machine learning in which PC value of location 1 is (0.31627, −0.26271), location 2 (0.31629, −0.03738), location 3 (0.31618, 0.1877), location 4 (0.31629, 0.18896), location 5 (0.31614, −0.53549), location 6 (0.31626, 0.24239), location 7 (0.31627, −0.24774), location 8 (0.31611, 0.47688), location 9 (0.31623, −0.34113), and normal phantom (0.31424, 0.3286). It has been clearly differentiated between without tumorous phantom and tumorous phantom, shown in Figure 6(b).

The experimental reflection coefficients of the antenna are collected by VNA using all three phantoms. The results of reflection coefficients due to normal phantom, single and multiple (two) tumor phantom are shown in Figure 6(c).

Figure 6(c) indicates that there is a very slight difference in reflection coefficients curves of normal phantom, phantom having single and phantom having multiple tumors. Therefore, to identify tumors

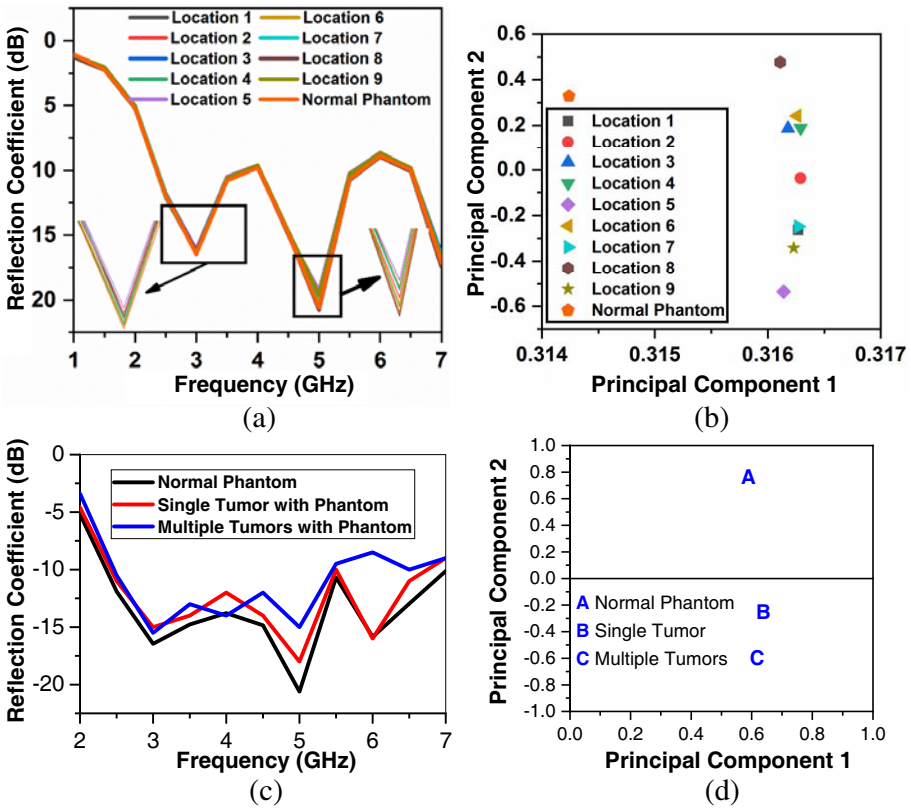

Figure 6. (a) Variations of the reflection coefficients with tumor located at fat and glandular in phantoms, (b) variations in the Principal Components with tumor located at fat and glandular in phantoms, (c) measurement of the reflection coefficients with phantoms, (d) measurement of Principal Components with phantoms.

correctly, PCA is used on these reflection parameters. The principal component values of normal and tumorous phantoms are analysed to differentiate them. For normal phantom, the PC-values are: (0.6, 0.75). For single tumor phantom, PC-values are: (0.62, −0.2). Similarly for multi-tumor phantom PC values are: (0.6, −0.6). Each phantom has different PC values. So due to different PC values, the tumor can be detected as shown in Figure 6(d). These results show the difference among the normal phantom, single tumor phantom, and multiple tumors.

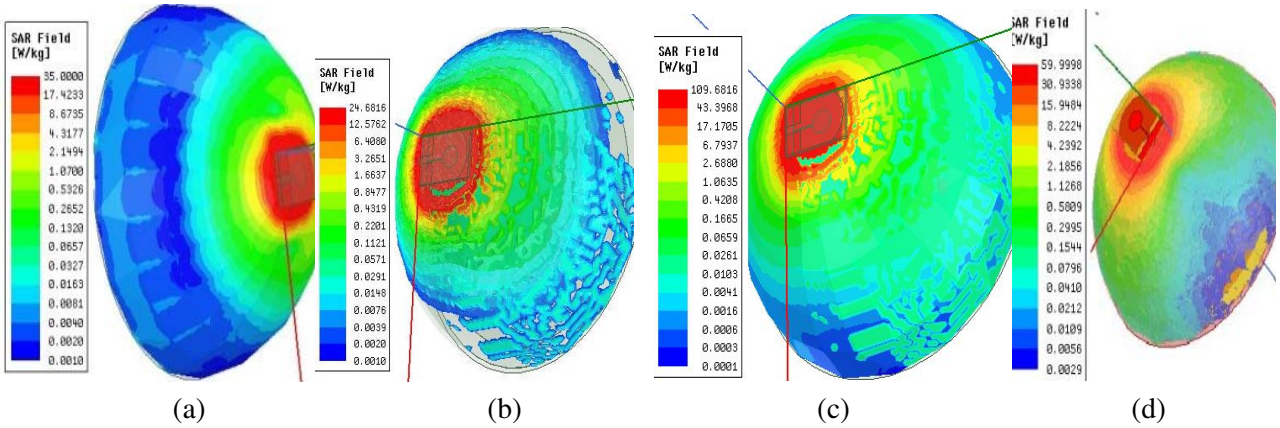

Figure 7. Simulated SAR value of breast model, (a) local SAR without tumor, (b) Avg SAR without tumor, (c) local SAR with tumor, (d) Avg SAR with tumor.

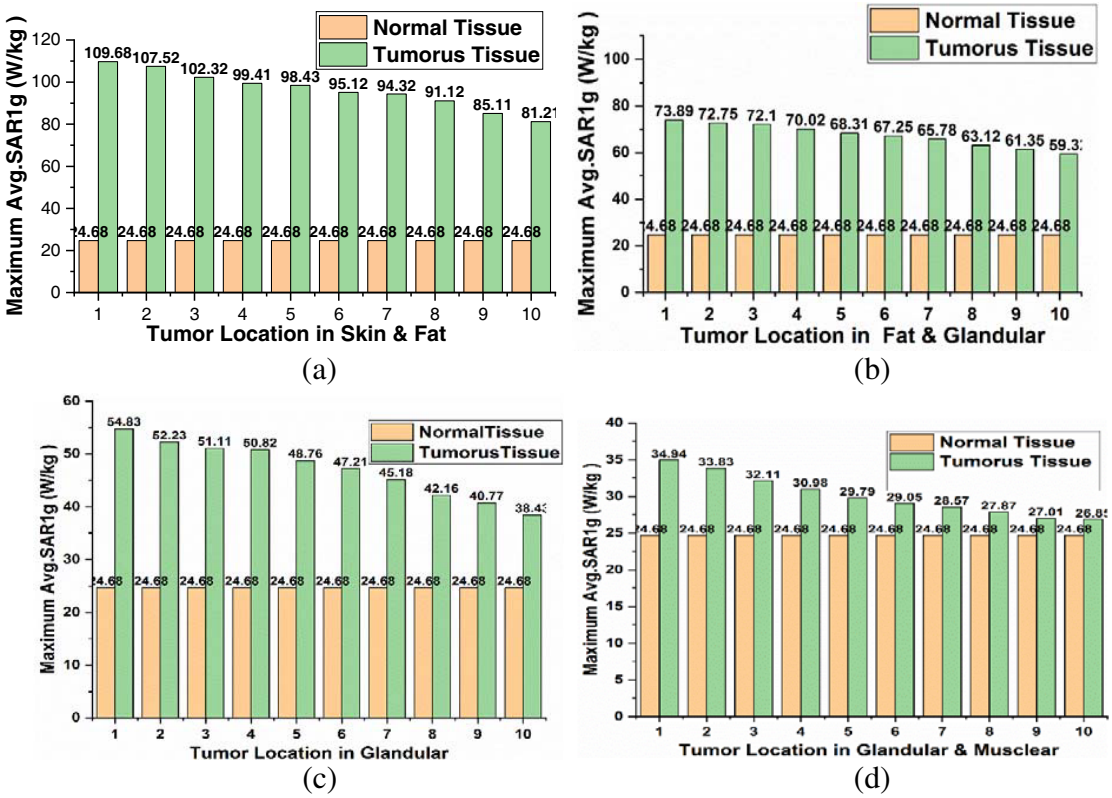

Figure 8. Simulated SAR value of breast model at different location, (a) tumor located at skin and fat, (b) tumor located at fat and glandular, (c) tumor located at glandular, (d) tumor located at glandular and Muscular.

4.2. Specific Absorption Rate

SAR is the amount of energy absorbed due to radio-frequency (RF) exposure by tissues in W/kg. The tissues' energy consumption is described in [29] and can be calculated in an average specific area (10 g or 1 g of tissue). The UWB antenna calculates the SAR1 g to spot the tumor. Here the tumor of radius 5 mm is introduced between skin and fat of breast phantom.

In the case of phantom without tumors, the maximum values of local and Avg SAR1 g are 35 W/kg and 24.68 W/kg, respectively, as show in Figures 7(a) & 7(b). Figures 7(c) & 7(d) show the SAR values for tumors phantom. The maximum values of local and Avg SAR are found 109.68 W/kg and 59.99 W/Kg, respectively, for a complete breast model with a tumor presented in Figures 7(c) & 7(d).

The maximum Avg SAR is calculated at different locations in different tissue layers. Figures 8(a), 8(b), 8(c), and 8(d) show the chart for the maximum Avg SAR value of normal tissue and tumors tissue at different tumor locations in different layers. This chart indicates that the Avg SAR values of cancerous tissue at a different locations in different tissue layers are much higher than normal tissue. Therefore, it clearly detects tumor location in a breast phantom.

Table 3 gives the comparison between the proposed antenna sensor and already reported antenna sensors.

Table 3. Comparison of proposed sensor with previous reported sensor for breast tumor detection.

Ref.	**Antenna size (mm^2)**	**Type of antenna**	**Experimental with**	**Antenna Port (Feed)**	**Result of sensor**
19	65.2×48	Cross-vivaldi	One oil phantom	Two	S_{11} analysis
20	19.36×27.72	Unit cell	CST based phantom	Two	Simulation based S_{11} analysis
21	200×200	Array	Carbon-rubber tissue phantom	Two	Switching S_{11} analysis
22	$25 \times 25 \times 25$	Co and Cross Vivaldi	HFSS phantom	Two	Simulation time analysis
24	35×30	Square ring shape	CST phantom	One	Simulated SAR
26	30×40	Four element based UMAS	Experimentally three phantoms	Four	S_{11} analysis using PCA
10	24×30.5	Resonator based notched behaviour Antenna	CST Phantom and Implement as sensor for tumor detection	Two	Imaging system development
23	24×30.5	Switchable filter antenna	CST Phantom		Imaging system development
Pro.	20×30	Circular resonator base antenna	Fabricated three heterogeneous phantom	One	S_{11} analysis using PCA and simulation SAR

5. CONCLUSION

A compact single radiating element antenna has been proposed for the detection of breast cancer. The antenna sensor operates within the 3.1 GHz to 6.8 GHz frequency range with a peak gain of 4.8 dB and peak radiation efficiency of 89.2%. Three different models of breast phantom have been developed for the experimental setup. The phantoms are of heterogeneous structures. From the measurement, it is

also evident that the electrical properties of the proposed phantom are very close to the real breast's electrical properties. The detection of cancerous tumors has been carried out by calculating the reflected power mismatch between the malignant and normal tissues with principal component analysis (PCA). Further SAR analysis is used to identify the location of tumors. Therefore, this sensor is useful for cancer detection.

ACKNOWLEDGMENT

This work is a part of a UPCST sponsored project with grant number CST/D-8326.

REFERENCES

1. Rao, P. K. and R. Mishra, "Elliptical shape flexible MIMO antenna with high isolation for breast cancer detection application," *IETE Journal of Research*, 1–9, 2020.
2. Kahar, M., A. Ray, D. Sarkar, and P. P. Sarkar, "An UWB microstrip monopole antenna for breast tumor detection," *Microwave and Optical Technology Letters*, Vol. 57, No. 1, 49–54, 2015.
3. Islam, M. T., et al., "A low cost and portable microwave imaging system for breast tumor detection using UWB directional antenna array," *Scientific Reports*, Vol. 9, No. 1, 1–13, 2019.
4. Kuhl, C. K., et al., "Mammography, breast ultrasound, and magnetic resonance imaging for surveillance of women at high familial risk for breast cancer," *Journal of Clinical Oncology*, Vol. 23, No. 33, 8469–8476, 2005.
5. Elmore, J. G., et al., "Ten-year risk of false positive screening mammograms and clinical breast examinations," *New England Journal of Medicine*, Vol. 338, No. 16, 1089–1096, 1998.
6. Sachs, J., et al., "Differential ultra-wideband microwave imaging: Principle application challenges," *Sensors*, Vol. 18, No. 7, 2136, 2018.
7. Islam, Md T., et al., "Microwave imaging based breast tumor detection using compact wide slotted UWB patch antenna," *Optoelectron. Adv. Mater. Rapid Commun.*, Vol. 13, 448–457, 2019.
8. Rao, P. K., A. R. Yadav, and R. Mishra, "AMC-based antenna sensor for breast tumors detection," *International Journal of Microwave and Wireless Technologies*, 1–8, 2020.
9. Saeidi, T., et al., "Ultra-wideband elliptical patch antenna for microwave imaging of wood," *International Journal of Microwave and Wireless Technologies*, Vol. 11, No. 9, 948–966, 2019.
10. Rahman, M., et al., "Resonator based switching technique between ultra-wide band (UWB) and single/dual continuously tunable-notch behaviors in UWB radar for wireless vital signs monitoring," *Sensors*, Vol. 18, No. 10, 3330, 2018.
11. Haider, Am., et al., "Time-domain investigation of switchable filter wide-band antenna for microwave breast imaging," *Sensors*, Vol. 20, No. 15, 4302, 2020.
12. Nejatijahromi, M., M. Rahman, and M. Naghshvarianjahromi, "Continuously tunable WiMAX band-notched UWB antenna with fixed WLAN notched band," *Progress In Electromagnetics Research Letters*, Vol. 75, 97–103, 2018.
13. NejatiJahromi, M., M. NagshvarianJahromi, and M. Rahman, "A new compact planar antenna for switching between UWB, narrow band and UWB with tunable-notch behaviors for UWB and WLAN applications," *Applied Computational Electromagnetics Society Journal*, Vol. 33, No. 4, 400, 2018.
14. Rahman, M., W. T. Khan, and M. Imran, "Penta-notched UWB antenna with sharp frequency edge selectivity using combination of SRR, CSRR, and DGS," *AEU-International Journal of Electronics and Communications*, Vol. 93, 116–122, 2018.
15. Rahman, M., et al., "Bandwidth enhancement and frequency scanning array antenna using novel UWB filter integration technique for OFDM UWB radar applications in wireless vital signs monitoring," *Sensors*, Vol. 18, No. 9, 3155, 2018.
16. Rahman, M., D.-S. Ko, and J.-D. Park, "A compact multiple notched ultra-wide band antenna with an analysis of the CSRR-TO-CSRR coupling for portable UWB applications," *Sensors*, Vol. 17, No. 10, 2174, 2017.

17. Rahman, M., et al., "Compact UWB band-notched antenna with integrated bluetooth for personal wireless communication and UWB applications," *Electronics*, Vol. 8, No. 2, 158, 2019.
18. Rahman, M. and J.-D. Park, "The smallest form factor UWB antenna with quintuple rejection bands for IoT applications utilizing RSRR and RCSRR," *Sensors*, Vol. 18, No. 3, 911, 2018.
19. Zhang, J., E. C. Fear, and R. H. Johnston, "Cross-Vivaldi antenna for breast tumor detection," *Microwave and Optical Technology Letters*, Vol. 51, No. 2, 275–280, 2009.
20. Islam, M. T., et al., "A negative index metamaterial-inspired UWB antenna with an integration of complementary SRR and CLS unit cells for microwave imaging sensor applications," *Sensors*, Vol. 15, No. 5, 11601–11627, 2015.
21. Foroutan, F. and N. K. Nikolova, "Active sensor for microwave tissue imaging with bias-switched arrays," *Sensors*, Vol. 18, No. 5, 1447, 2018.
22. Jafari, H. M., J. M. Deen, S. Hranilovic, and N. K. Nikolova, "Co-polarised and cross-polarised antenna arrays for breast, cancer detection," *IET Microwaves, Antennas & Propagation* Vol. 1, No. 5, 1055–1058, 2007.
23. Haider, A., et al., "Time-domain investigation of switchable filter wide-band antenna for microwave breast imaging," *Sensors*, Vol. 20, No. 15, 4302, 2020.
24. Subramanian, S., B. Sundarambal, and D. Nirmal, "Investigation on simulation-based specific absorption rate in ultra-wideband antenna for breast cancer detection," *IEEE Sensors Journal*, Vol. 18, No. 24, 10002–10009, 2018.
25. Amdaouch, I., O. Aghzout, A. Naghar, A. V. Alejos, and F. J. Falcone, "Breast tumor detection system based on a compact UWB antenna design," *Progress In Electromagnetics Research M*, Vol. 64, 123–133, 2018.
26. Sharma, M. K., et al., "Experimental investigation of the breast phantom for tumor detection using ultra-wide band–MIMO antenna sensor (UMAS) probe," *IEEE Sensors Journal*, Vol. 20, No. 12, 6745–6752, 2020.
27. Rahman, M. and J. D. Park, "The smallest form factor UWB antenna with quintuple rejection bands for IoT applications utilizing RSRR and RCSRR," *Sensors*, Vol. 18, 911, 2018.
28. Rahmana, M., W. T. Khana, and M. Imran, "Penta-notched UWB antenna with sharp frequency edge selectivity using combination of SRR," *CSRR, and DGS. Int. J. Electron. Commun.*, Vol. 93, 154–157, 2016.
29. Garg, R., P. Bhartia, I. J. Bahl, and A. Ittipiboon, *Microstrip Antenna Design Handbook*, Artech House, 2001.
30. Islam, Md T., et al., "Experimental breast phantoms for estimation of breast tumor using microwave imaging systems," *IEEE Access*, Vol. 6, 78587–78597, 2018.